Quaternary Science Reviews 27 (2008) 2292–2302

Contents lists available at ScienceDirect

Quaternary Science Reviews

journal homepage: www.elsevier.com/locate/quascirev

Searching for eustasy in deglacial sea-level histories

Glenn A. Milne [a,*], Jerry X. Mitrovica [b]

[a] Department of Earth Sciences, University of Ottawa, Canada
[b] Department of Physics, University of Toronto, Canada

ARTICLE INFO

Article history:
Received 20 December 2007
Received in revised form 20 August 2008
Accepted 22 August 2008

ABSTRACT

Perturbations to the Earth's gravity field and solid surface associated with glacial isostatic adjustment (GIA) cause the total (observable) sea-level change to depart from the eustatic curve, which is defined as a spatially uniform height shift of the ocean surface to accommodate any mass gained/lost from grounded ice. In this study we apply a state-of-the-art model of GIA-induced sea-level change to quantify the magnitude and spatial form of this departure at the global scale for a range of model parameters with an aim to identify regions that are well suited to obtain accurate and precise estimates of eustatic sea level (and therefore past grounded ice volume). In general, our results indicate that eustatic sea level is not a directly measurable quantity and so must be estimated by subtracting a model-derived estimate of non-eustatic contributions from observations. In this regard, we use our results to isolate regions where this procedure can be applied with optimal accuracy and precision. That is, where (1) the GIA predictions are relatively insensitive to plausible ranges in input parameters and (2) where the non-eustatic contribution is small (i.e., the predicted sea level closely approximates the eustatic value). We present maps that can be employed by the field community to identify areas where sea-level reconstructions would be well suited to arrive at robust estimates of eustatic sea level. Note that sea-level changes associated with tectonic motion and changes in ocean water temperature/salinity, which also lead to departures from eustasy, are not considered in this analysis.

1. Introduction

At most localities around the globe, mass exchange between ice sheets and oceans and the consequent response of the solid Earth and the gravity field to this exchange are the processes that dominated sea-level changes during the Quaternary. The growing observational database demonstrates the distinct spatial variation of this glaciation-induced sea-level signal. For example, following the last glacial maximum (LGM), a monotonic sea-level fall is observed in regions near the centre of the largest ancient ice sheets (e.g. so-called "near-field" regions such as Canada and Fenno-scandia), whereas a monotonic sea-level rise is commonly observed until the mid-Holocene in regions removed from major glaciation centres (e.g. "far-field" sites such as Barbados). These end-member scenarios bound a complex spectrum of relative sea-level (RSL) signatures that reflect the interactions between ice sheets, oceans and the solid Earth.

Observations of RSL during the late Quaternary, particularly for the post-LGM period, have been employed in a number of important applications. Since the observed RSL signal in near-field regions is dominated by the isostatic response of the solid Earth to the local ice unloading, these data are commonly used to constrain models of ice history and Earth viscosity structure (e.g. Haskell, 1935; Peltier and Andrews, 1976; Wu and Peltier, 1983; Tushingham and Peltier, 1991; Lambeck, 1993; Mitrovica and Peltier, 1993; Mitrovica, 1996; Lambeck et al., 1998; Shennan et al., 2002; Peltier, 2004). The observed RSL signal in far-field regions has also been used to infer mantle viscosity structure (e.g. Nakada and Lambeck, 1989). However, since this signal is dominated by the influx of glacial meltwater to the oceans, the more common application of far-field observations has been to constrain volumetric changes in global grounded ice as a function of time (e.g. Nakada and Lambeck, 1989; Peltier, 1994, 2002; Fleming et al., 1998; Yokoyama et al., 2000; Lambeck, 2002; Lambeck et al., 2002; Milne et al., 2002, 2005; Lambeck et al., 2004; Peltier and Fairbanks, 2006). It is the second of these applications that is the focus of this study.

At tectonically stable far-field locations, the observed sea-level rise is commonly taken to be a good approximation of the glacio-eustatic component of sea-level change (hereafter referred to as the eustatic component). This component is defined as a globally uniform height shift of the ocean surface that would occur (in the absence of gravitational effects and Earth deformation) due to mass input from continental ice reservoirs (e.g. Farrell and Clark, 1976). If we assume that oceans are bounded by steep cliffs, so that changes

* Corresponding author.
E-mail address: gamilne@uottawa.ca (G.A. Milne).

0277-3791/$ – see front matter © 2008 Elsevier Ltd. All rights reserved.
doi:10.1016/j.quascirev.2008.08.018

in local sea level do not produce on-lap or off-lap of water (i.e., the shorelines are fixed in time), the eustatic sea-level change can be expressed quantitatively as

$$S_{\mathrm{eus}}(t) = -\frac{\rho_{\mathrm{ice}}}{\rho_{\mathrm{water}}}\left[\frac{V_{\mathrm{ice}}(t) - V_{\mathrm{ice}}(t_0)}{A_{\mathrm{ocean}}(t_0)}\right] \quad (1)$$

where S_{eus} is the eustatic shift of the ocean surface relative to present; $V_{\mathrm{ice}}(t)$ is global grounded ice volume at some time in the past (t) and $V_{\mathrm{ice}}(t_0)$ is the value at present (t_0); $A_{\mathrm{ocean}}(t_0)$ is the area of the ocean at present and ρ_{ice} and ρ_{water} are, respectively, the densities of ice and water. Eq. (1) is a statement of mass conservation in which any mass lost/gained by grounded ice is gained/lost by the oceans. It follows that an estimate of eustatic sea-level change can provide a direct measure of past global ice volume, which is a useful constraint on models of global ice extent during the late Quaternary and an independent measure with which to calibrate marine oxygen isotope records.

A more accurate version of Eq. (1) is written in integral form to account for the time variation in ocean area over a given period (e.g. Lambeck et al., 2000). In the case of a time-dependent shoreline, Eq. (1) is extended to

$$S_{\mathrm{eus}}(t) = -\frac{\rho_{\mathrm{ice}}}{\rho_{\mathrm{water}}}\int_{t_0}^{t}\frac{\dot{V}_{\mathrm{ice}}(t)}{A_{\mathrm{ocean}}(t)}\mathrm{d}t \quad (2)$$

where $\dot{V}_{\mathrm{ice}}(t)$ is the time rate of change in global grounded ice volume.

A number of early studies adopted the assumption that the observed sea-level change would closely approximate the eustatic component in regions that were tectonically stable and sufficiently distant from previously glaciated regions and so set out to determine a reference global eustatic curve (e.g. Milliman and Emery, 1968). Subsequent to this time, however, a growing database of increasingly more accurate and precise post-LGM observations as well as advances in modelling glaciation-induced sea-level change, have demonstrated that this view is overly simplistic.

There are a number of processes that cause glaciation-induced sea-level changes to depart from the eustatic value. Sea level can be perturbed via vertical deflections of either the ocean floor or the ocean surface. It is well known that the ocean floor is deflected due to the isostatic response of the solid Earth to the changing ice and ocean water mass distributions associated with the glacial cycles (e.g. Daly, 1925; Bloom, 1967; Chappell, 1971). The ocean surface is also perturbed due to the gravitational attraction between ice sheets and ocean water, and ocean water with itself (e.g. Woodward, 1888; Clark, 1976), and the gravitational attraction between the (deforming) solid Earth and ocean water.

In a landmark paper, Farrell and Clark (1976) incorporated these physical processes into a formal theory of glaciation-induced sea-level change that can be expressed as a single, integral equation (known as the "sea-level equation"). Solving this equation permits accurate predictions of sea-level change for a prescribed ice loading history and a model of Earth density and rheology structure. An early application of the sea-level equation by Clark et al. (1978) demonstrated that the predicted post-LGM sea-level change deviates significantly from the eustatic component even in far-field regions. Indeed, their results led the authors to conclude that "There are no "stable" regions where eustatic sea level can be measured" (p. 286) and that the eustatic signal must be *inferred* by comparing model predictions to observations.

In the present paper we revisit the issue addressed by Clark et al. (1978). Specifically, we apply a state-of-the-art model of sea-level change to consider, explicitly, the deviation between the predicted sea-level change and the eustatic component of this change. In particular, we wish to quantify the deviation from the eustatic value in far-field regions to aid field scientists in selecting optimal sites to obtain robust estimates of eustatic sea-level change (and therefore past grounded ice volume). It is quite possible that, in certain areas, the various contributing processes nearly cancel each other so that the net signal is very close to the eustatic value for at least a part of the post-LGM period.

Models of glaciation-induced sea-level change have improved dramatically in the past few decades. The original sea-level theory derived by Farrell and Clark (1976) and applied by Clark et al. (1978) has been extended to incorporate a variety of effects, such as: lateral shifts in shoreline position associated with local changes in sea level (e.g. Johnston, 1993; Peltier, 1994; Milne et al., 1999); the growth and retreat of marine-based ice sheets (Milne, 1998; Peltier, 1998; Milne et al., 1999); and the feedback of glaciation-induced perturbations in Earth rotation (e.g. Milne and Mitrovica, 1996). Milne (2002) provides a review of these more recent advances. Moreover, Mitrovica and Milne (2003) derived a generalised theory that incorporates each of the above extensions, and have also assessed the relative accuracy of previous treatments (see also Kendall et al., 2005). These analyses demonstrated that shoreline migration and rotation signals can have a significant impact on the predictions of post-LGM sea-level changes in specific regions.

We begin the next section with a brief description of the theory and models adopted in this study. We then go on to examine predictions based on a single ice–Earth model combination to consider the deviation of the total predicted signal from the eustatic value and provide a brief discussion of the physical mechanisms responsible for this deviation. We consider sea-level change over two time windows extending to the present-day: the first from LGM (21 cal. kyr BP) and the second from the mid-Holocene (6 cal. kyr BP). These choices are motivated by the importance of obtaining accurate constraints on grounded ice volume at these times (e.g. Clark and Mix, 2002; Lambeck, 2002). We then proceed in Section 2.2 to focus on the objective of locating regions well suited to obtaining a robust estimate of ice volume. Specifically, we seek sites where: (i) the total RSL signal is close to the eustatic component and (ii) the difference between these quantities is relatively insensitive to plausible variations in input model parameters, particularly Earth viscosity structure. Identifying such sites ensures that the common procedure of 'correcting' the observations to infer the eustatic signal is robust.

2. Modelling results

The sea-level model we apply requires two inputs: a space-time history of large-scale grounded ice distribution during the most recent glacial cycle and parameters defining a one-dimensional, visco-elastic Earth model. Once these inputs are defined we compute the corresponding sea-level change by solving the sea-level equation described in Mitrovica and Milne (2003) using the algorithm (for 1-D Earth models) outlined in Kendall et al. (2005). We predict GIA perturbations in Earth rotation using the revised theory described in Mitrovica et al. (2005), and the feedback of this effect on sea-level change is computed using the theory described in Milne and Mitrovica (1996).

Two distinct ice models are considered to demonstrate the sensitivity of predictions to the input ice history. The first is based on the ICE3G model (which describes ice evolution following the LGM only; Tushingham and Peltier, 1991) and has been altered significantly to include a glaciation phase and to provide a good fit to far-field observations from Barbados, Huon Peninsula, Tahiti and the Sunda Shelf (Bassett et al., 2005). A key aspect of this model is that it contains a large Antarctic contribution to the rapid sea-level rise observed at ~14 cal. kyr BP (so-called Meltwater Pulse IA; Fairbanks, 1989; Bard et al., 1990). The second is the ICE-5G model

(e.g. Peltier, 2004), which has been tuned to fit a variety of GIA-related observables; in this model, Meltwater Pulse IA is sourced entirely from northern hemisphere ice sheets (primarily the North American ice sheets).

The Earth model we employ is a spherically symmetric, self-gravitating Maxwell visco-elastic body. The elastic and density structure are taken from seismic constraints (Dziewonski and Anderson, 1981). The values adopted are depth parameterised by volume averaging PREM (Preliminary Reference Earth Model) into shells with thickness of 10.5 km in the crust and 25 km in the mantle. In most of the viscosity models we consider, the depth variation of this parameter is more crudely parameterised: an outer shell of very high viscosity to simulate an elastic lithosphere, and two deeper regions of uniform viscosity beneath the model lithosphere. The first of these regions extends to the 660 km deep seismic discontinuity (the upper mantle) and the second from this depth to the core-mantle boundary (the lower mantle).

In the following analysis, a range of results are generated by varying the viscosity within the model upper and lower mantle regions and the thickness of the model lithosphere. In principle, each of the adopted ice models should be partnered with the Earth viscosity model that resulted in the best fit to the data considered. The Bassett et al. (2005) ice model produced the best fit to the far-field sea-level data for an Earth model with a lower mantle viscosity of 4×10^{22} Pas (the fit was insensitive to a range of values considered for lithospheric thickness and upper mantle viscosity). The ICE-5G ice model gives optimal results in most locations when coupled to the VM2 Earth viscosity model. This viscosity model, which contains greater depth resolution than described above, includes a 90 km thick lithosphere and is characterised by a moderate increase in viscosity within the lower mantle, from $\sim 2 \times 10^{21}$ Pas in the shallowest layers to $\sim 3 \times 10^{21}$ Pas at the CMB (see Fig. 1 in Peltier, 2004).

It is important to note that the predictions do not take into account any tectonic processes and so the results shown below are only applicable to regions that are tectonically stable or to data sets that have been corrected for this signal. In addition, the influence of ocean density (steric) changes is not considered.

2.1. Departures from eustasy

We begin by showing, in Fig. 1, a plot of predicted relative sea-level (RSL) for 21 cal. kyr BP (A) and 6 cal. kyr BP (B). That is, these are global predictions of the present elevation of sea-level indicators from this age. To emphasise departures from eustasy, the results are shown relative to the eustatic sea level for the same ages (-127 m and -1 m, respectively.) The model eustatic value was computed using Eq. (2). As a companion to this figure, Fig. 2 shows the full post-LGM time history predicted for two sites: Richmond Gulf (Hudson Bay) and Tahiti (see Fig. 1). The latter site is commonly considered to be within the far-field of the Late Pleistocene ice sheets, while the former is in the near-field of the Laurentide ice sheet.

The results in Fig. 1A indicate that there are significant deviations from the eustatic value (>10 m) even at low latitudes and that the departure from eustasy has a spatial variation that is highly complex. In the following paragraphs we highlight the main features evident in Fig. 1 and outline the processes responsible for them.

Not surprisingly, the largest deviations from the eustatic value occur in broad regions centred on the locations of former and present ice sheets. In particular, sea levels are predicted to have been higher than the eustatic value within the majority of the northern hemisphere. The prediction for Richmond Gulf in Fig. 2 is a classic example of a near-field sea-level curve: the uplift of the solid Earth in response to Laurentian ice melting (i.e., post-glacial rebound) yields a RSL for the LGM of ~ 450 m. The associated eustatic value for 21 cal. kyr BP is -127 m, and thus the discrepancy reaches ~ 577 m at this site (which is well above the colour scale in Fig. 1). There are two effects associated with the ice loading that are primarily responsible for such large and positive departures from eustasy in near-field regions: the isostatic depression and subsequent uplift of the solid Earth, and the reduction in the broad ocean surface high due to the loss of gravitational attraction between ocean water and the ice sheets. The latter, so-called direct effect has been recognised for some time (e.g. Woodward, 1888), and, in the case of sea-level change in response to rapid melting, it forms the basis of the relatively recent method of 'sea-level fingerprinting' to infer melt distribution from sea-level observations. (e.g. Mitrovica et al., 2001; Clark et al., 2002). In any event, it is interesting to note that, in all but a few isolated regions (e.g. the Labrador and Norwegian Seas), these two effects dominate for this particular

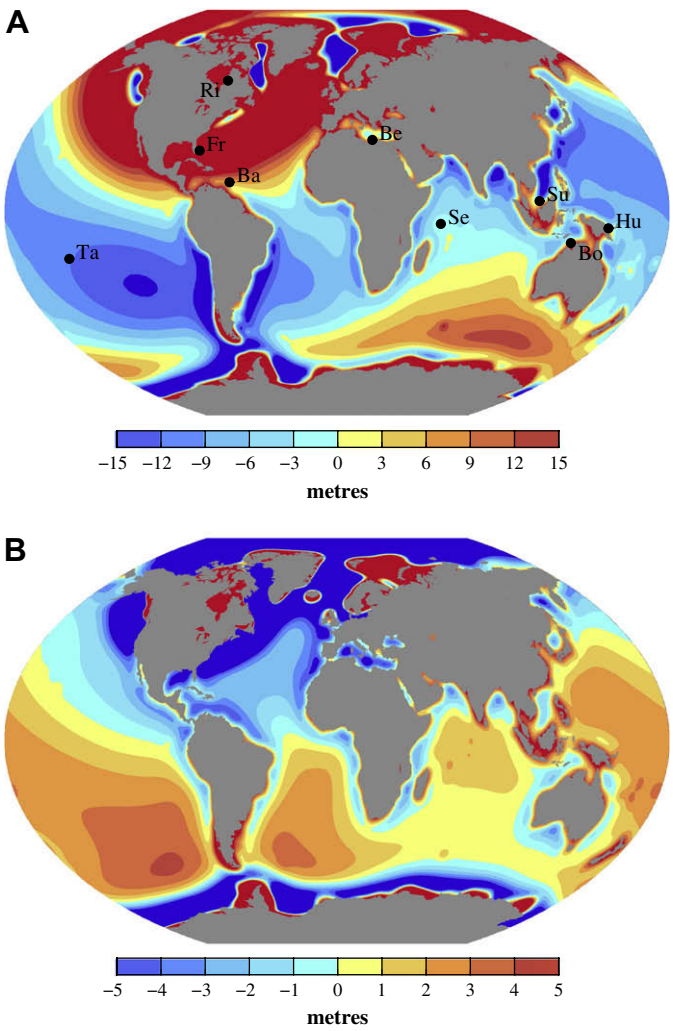

Fig. 1. Predicted total RSL change minus the model eustatic component for a time window extending from either 21 cal. kyr BP (A) or 6 cal. kyr BP (B) to the present-day. The prediction is based on the Bassett et al. ice model and the associated Earth model that provides an optimal fit to a suite of far-field observations (see main text for details). The zero contour marks where the total RSL is equal to the model eustatic value, with red and blue colours indicating sea levels that are, respectively, above and below the eustatic value. Note that the darkest red and blue colours indicate regions where the departure from eustatic sea level is greater that 15 m (A) and 5 m (B) (these colours are not shown on the colour bar). Locations of sites referred to in this paper are shown (from west to east these are: Tahiti (Ta), Freeport (Fe), Richmond Gulf (Ri), Barbados (Ba), Benghazi (Be), Seychelles (Se), Sunda Shelf (Su), Bonaparte Gulf (Bo) and Huon Peninsula (Hu)). (For interpretation of the references to colour in this figure legend, the reader is referred to the web version of this article.)

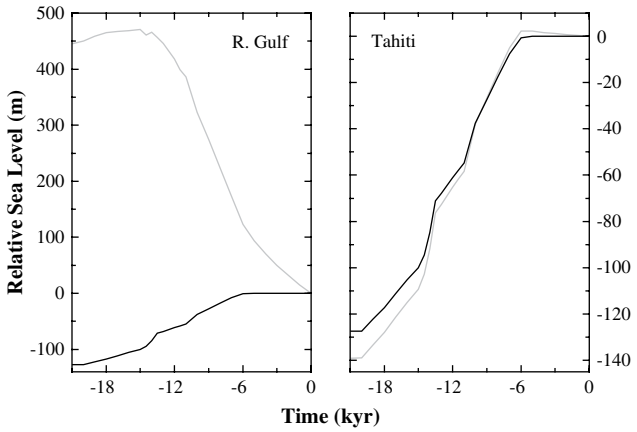

Fig. 2. Predicted RSL histories (grey lines) at Richmond Gulf and Tahiti (see Fig. 1). The calculations are based on the Earth and ice model specified in the caption to Fig. 1 (see also main text). The black lines (which are identical for each frame) represent the eustatic sea-level variation since the LGM.

ice–Earth model combination. Within this zone, sea-level indicators of LGM age are predicted to be higher than the eustatic level. The isolated regions which display LGM sea levels below the eustatic value are found in areas where the subsidence of the ocean floor is greater than the sea-surface fall associated with gravitational effects.

The large amplitude deviation from the eustatic value surrounding the Antarctic continent is driven by the same processes as in the near-field northern hemisphere regions. The spatial extent of the elevation relative to the eustatic level is significantly more limited in the southern hemisphere due, in part, to the relatively small volume of post-LGM ice loss compared to the northern hemisphere in the Bassett et al. model (~25 m eustatic equivalent in the south compared to ~100 m in the north).

The broad band of blue contours in Fig. 1A, located in the southern hemisphere near South America and ranging to more northerly latitudes near Africa and into the western Pacific, largely reflects the post-LGM sea-level rise associated with the direct gravitational effect discussed above. That is, the migration of water away from the ablating high latitude ice masses yields a RSL for LGM that is lower than the eustatic elevation within this band (e.g. Tahiti; see Fig. 2). The greater proportion of grounded ice in the northern hemisphere at the LGM is the primary reason that the mean location of this band is within the southern hemisphere.

At low-to-mid latitudes, in regions more distant from the major glaciation centres, sea levels generally lie within 12 m of the eustatic value. The influence of hydro-isostasy (water loading) and GIA-induced perturbations in Earth rotation are more evident at these latitudes. The hydro-isostatic effect of continental levering – a flexure of the lithosphere due to ocean loading near continental margins (e.g. Clark et al., 1978; Nakada and Lambeck, 1989) – causes an uplift of the solid Earth around and within land areas from the

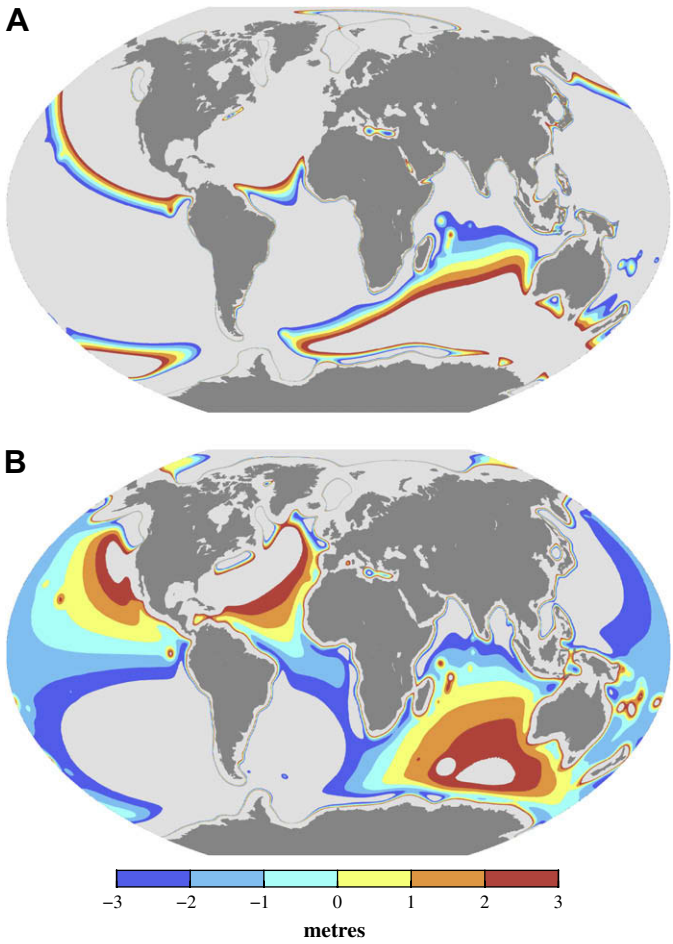

Fig. 3. (A) Same as Fig. 1A except that contour range is restricted to ±3 m. (B) Same as (A) except that results calculated using the ICE-5G/VM2 (90 km lithosphere) ice–Earth model combination (Peltier, 2004).

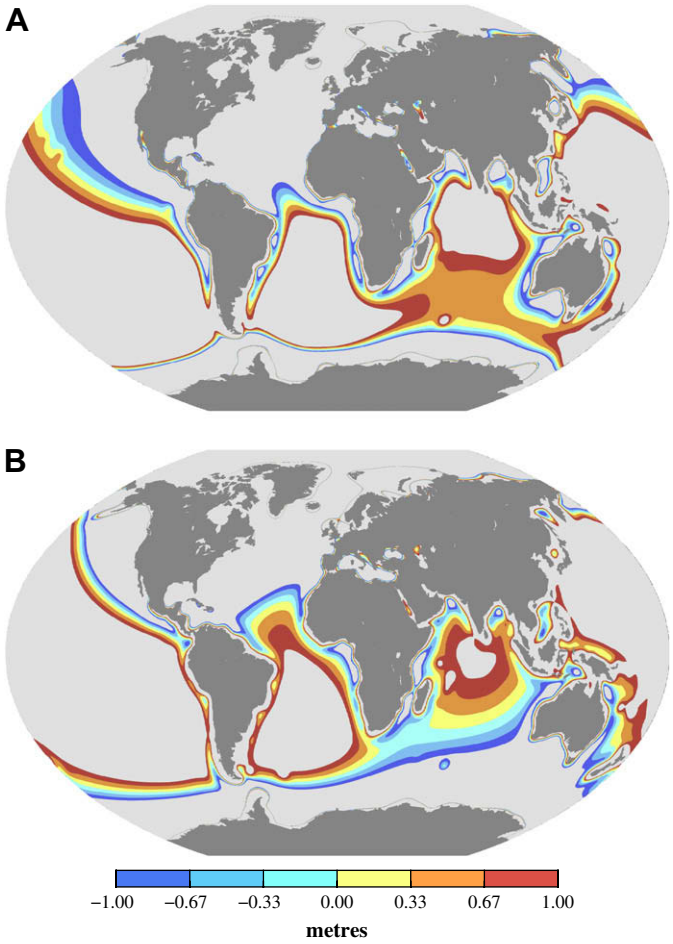

Fig. 4. (A) Same as Fig. 1B except that contour range is restricted to ±1 m. (B) Same as (A) except that results calculated using the ICE-5G/VM2 (90 km lithosphere) ice–Earth model combination (Peltier, 2004).

LGM to present, resulting in a RSL for the LGM that is higher than the eustatic value. This effect, which produces the thin red halo surrounding the continents in Fig. 1A, is most pronounced in areas surrounded by extensive and shallow continental shelf that was gradually inundated during deglaciation.

The influence of Earth rotation on sea level is due to a perturbation of the rotation vector associated with large-scale glaciation (e.g. Sabadini et al., 1982; Wu and Peltier, 1984; Mitrovica et al., 2005). One aspect of this perturbation leads to motion of the rotation pole relative to the solid Earth. This so-called 'True Polar Wander' results in a pole tide effect which causes deformation of the solid Earth and gravity field at very long-wavelengths and displays a characteristic four-quadrant pattern (e.g. Milne and Mitrovica, 1998). This process acts to produce a net rise in post-LGM sea level around South America, China and Japan and a net fall in sea levels around southwestern Australia and North America (see Fig. 1A). That is, within the former zones, the rotational feedback contributes to a RSL for LGM that is lower than the eustatic level (e.g. Tahiti, where the effect acts in concert with water migration associated with the direct gravitational attraction of the ablating ice loads described above; Fig. 2) and an opposite contribution within the latter (antipodal) zones. The rotation signal gives rise to the distortion of the broad band of (sub-eustatic) blue contours in Fig. 1A (more southerly near South America and more northerly in the western Pacific). Moreover, the rotation effect adds to the continental levering signal in Australia but opposes this signal in South America.

Next, we consider the global map of RSL for 6 cal. kyr BP relative to the model eustatic level at this time ($\sim$1 m). Comparison of these results (Fig. 1B) to those in Fig. 1A shows that there are distinct differences in the spatial patterns predicted for these two ages, and so optimal locations for estimating the eustatic signal during the LGM may not be optimal for other time windows. The extensive region of high sea levels (relative to the eustatic component) in the northern hemisphere at the LGM (Fig. 1A) has retreated to exist only in areas undergoing crustal uplift due to ice unloading. The majority of this region now exhibits sea levels that are considerably lower than the eustatic value due to peripheral bulge subsidence (and sea-level rise) between this time and the present. The dramatic change in this region between the LGM and mid-Holocene is a consequence of all major ice sheets having melted; thus, the long-wavelength reduction in gravitational attraction between the ablating major northern hemisphere ice sheets (in North America, Eurasia) and the ocean evident in Fig. 1A is no longer active in Fig. 1B.

At lower latitudes, the mid-Holocene signal is, again, dominated by the influence of hydro-isostasy and rotation effects. Note, however, that the broad band of blue in Fig. 1A has been replaced by a yellow–red band that signifies a RSL for 6 cal. kyr BP that is higher than the eustatic level. There are two reasons for this change in sign, which reflects a net fall in sea level over the last 6 cal. kyr within this region (once again, an example is Tahiti in Fig. 2). First, the sign of the rotation-induced signal is reversed compared to that in Fig. 1A. The rotation signal is predicted to change sign during the Late Glacial ($\sim$12 cal. kyr BP) when the solid surface height shift due to the rotational forcing becomes dominant over the sea-surface perturbation at this time (e.g. see Fig. 5 in Milne and Mitrovica, 1998). Second, a process termed "ocean syphoning" (Mitrovica and Peltier, 1991; Mitrovica and Milne, 2002), in which water migrates from the far-field ocean basins to accommodate regions of sea-level rise (blue zones) at the periphery of glaciation centres and offshore of continents, contributes a broad fall in sea level within these ocean basins throughout the post-LGM period (Milne et al., 2002).

Ocean syphoning also influences the results in Fig. 1A but, in this case, it is being swamped by the contribution from the direct gravitational attraction effect associated with the ablating ice sheets. The absence of the latter effect in Fig. 1B is also the reason why the sea-level rise offshore of low latitude continental margins associated with continental levering (e.g. around South America, southern Africa and Australia) becomes obvious. (This offshore signal is evident in Fig. 1A through a slightly enhanced sea-level rise around the same continents.) Finally, Fig. 1B indicates that RSL for 6 cal. kyr BP at Huon Pensinsula is particularly high relative to the eustatic level. As in the case of Tahiti, this is partly due to a sea-level fall associated with rotational effects and ocean syphoning. However, the location of this site on a shallow continental shelf means that it is also subject to a sea-level fall due to continental levering. The net effect is a pronounced highstand predicted at this site for a 6 cal. kyr BP sea-level indicator.

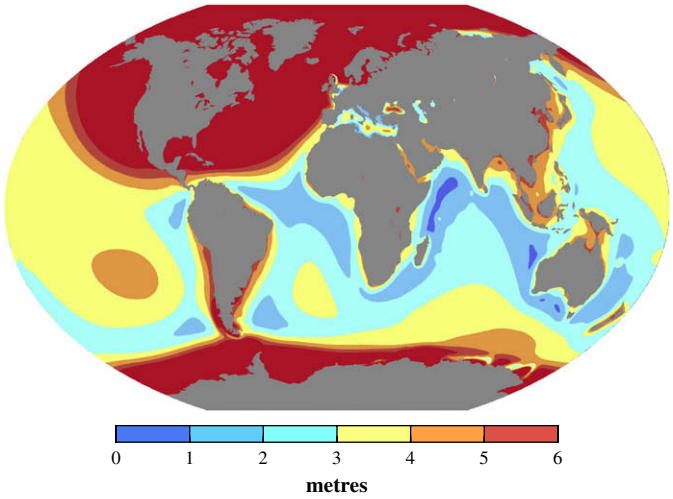

Fig. 5. Standard deviation of predicted RSL for the LGM (21 cal. kyr BP) generated using the Bassett et al. ice model and a suite of 162 Earth viscosity and lithospheric thickness models (see text for details). Blue colours denote areas where predictions display low sensitivity to plausible variation in Earth model parameters. Values over 6 m are indicated by the darkest red colour (not shown on colour bar).

2.2. Optimal locations to infer the eustatic component of sea level

The predictions shown in Fig. 1 (A and B) illustrate the complexity of glaciation-induced sea-level change. Moreover, they demonstrate that the total signal deviates substantially from the eustatic value at most locations, even sites within the far-field of the past and present ice sheets. The results shown in Fig. 3A are the same as those in Fig. 1A except that regions where the absolute difference between RSL and the eustatic signal is greater than 3 m are shown in light grey. A bound of $\pm$3 m was chosen to reflect the level of precision available from different types of high-quality sea-level indicators previously applied to reconstruct LGM sea levels (e.g. Fairbanks, 1989; Hanebuth et al., 2000; Yokoyama et al., 2000). In Fig. 3A, the 'band' of locations where the total RSL signal lies within 3 m of the eustatic value is spatially limited. Note that there are regions, such as the Indian Ocean, where this band is quite extensive due to the relatively low spatial gradients in the predicted sea-level signal. In contrast, there are a number of other areas where the band is narrow due to the large gradient associated with glacio- or hydro-isostasy. A rather extreme example of the latter are the thin zones that encircle continental margins in the far-field of the Late Pleistocene ice sheets (e.g. around South America, Africa and Australia). The narrowness of these zones reflects the gradient in the signal associated with continental levering (Fig. 1A), and they are displaced from the present-day shoreline by a distance which is

a function of the width of the local continental shelf. As a consequence of the levering process, there are a limited number of locations along the coasts of large land masses (dimension greater than a few hundred km) where the measured RSL will be close to the eustatic value.

The results shown in Figs. 1 and 3A are based on a single ice–Earth model combination tuned to fit data from selected far-field locations (Bassett et al., 2005). In Fig. 3B we show results analogous to Fig. 3A generated using an alternative GIA model that is comprised of the ICE-5G ice history and the companion VM2 Earth viscosity model with a 90 km thick lithosphere (e.g. Peltier, 2004). There are large differences between the two sets of predictions: in particular, the ICE-5G/VM2 model predicts a significantly more extensive area in which LGM sea levels are within 3 m of the eustatic value. There are a number of differences between the two GIA models considered that could account for the discrepancy between Fig. 3A and B. Most notable amongst these are the contrasting scenarios for the source of Meltwater Pulse IA and the viscosity within the lower mantle (this viscosity ranges from 0.9 to 4×10^{21} Pas in the VM2 model and is 40×10^{21} Pas in the Bassett et al. model). Additional model runs (see next Section) demonstrate that it is the contrasting values of lower mantle viscosity that accounts for the majority of the differences evident between the frames in Fig. 3.

In Fig. 4 we show predictions based on the same two GIA models considered in Fig. 3, but for the time 6 cal. kyr BP. In this case, a range of ± 1 m relative to the eustatic value was chosen to reflect the precision of high-quality sea-level indicators adopted for reconstructing mid-Holocene sea levels (e.g. van de Plassche, 1986). The difference between the results in Fig. 4A and B, again, primarily a consequence of the contrasting values of lower mantle viscosity, is much reduced compared to those at the LGM. However, these differences remain significant and so we conclude that the current level of uncertainty in GIA models, both in terms of Earth viscosity structure and, to a lesser extent, Late Pleistocene ice history, preclude the use of a single combination ice–Earth model to generate an accurate and definitive global map of RSL relative to the eustatic value.

It may, nevertheless, be possible to isolate specific geographic sites which do provide a robust measure of the eustatic trend, and this issue serves as the focus of the remainder of this study. To this end, we have extended the above results to consider a large suite of plausible three-layer viscosity models. Specifically, for each of the two ice models discussed above, we generated predictions for 162 Earth models that explore all possible permutations of the following parameter values: (i) lithospheric thickness: 71, 96, 120 km; (ii) upper mantle viscosity: 1, 2, 3, 5, 8, 10×10^{20} Pas; and lower mantle viscosity: 1, 2, 3, 5, 8, 10, 20, 30, 50×10^{21} Pas. The ranges of these parameter values reflect the end-member variability when considering the results obtained in different global and regional GIA analyses (e.g. Nakada and Lambeck, 1989; Kaufmann and Lambeck, 2002; Peltier, 2004; Mitrovica and Forte, 2004).

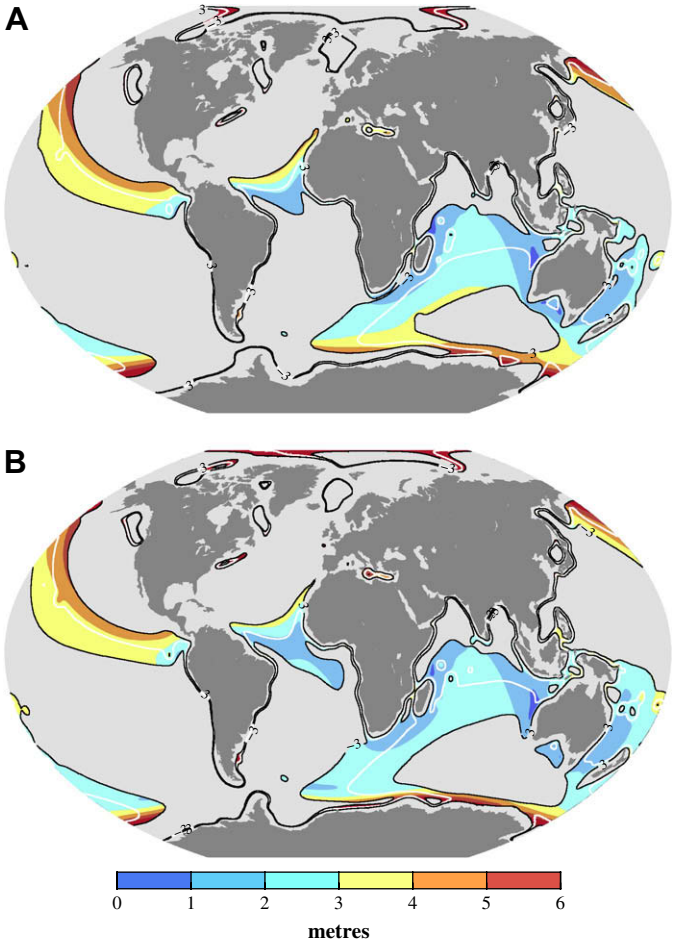

Fig. 6. (A) Same as Fig. 5 except that standard deviations are only plotted within regions in which the mean RSL prediction for the ensemble lies within 3 m of the mean eustatic value. The white contour indicates where these values are the same. (B) As in (A) with the exception that results are shown for the ICE-5G ice history.

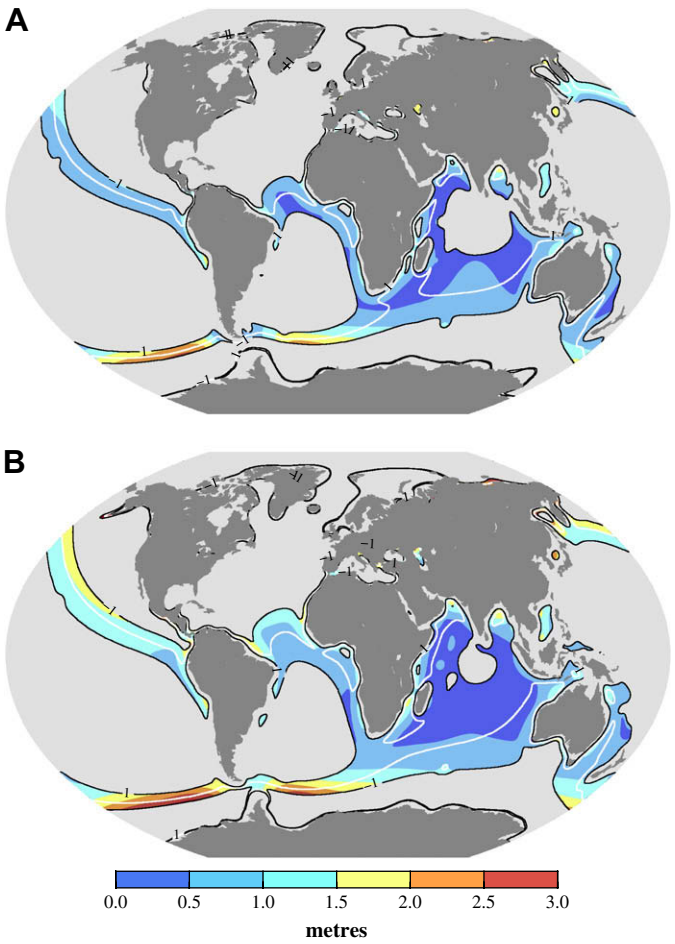

Fig. 7. Same as Fig. 6 but for mid-Holocene (6 cal. kyr BP) RSL predictions. Frames A and B denote results for the Bassett et al. and ICE-5G models, respectively. In this case the results are limited to zones in which the mean of the RSL predictions lies within 1 m of the mean eustatic value.

Using this ensemble of model runs, we first computed the mean eustatic value for a given ice model at the two times considered in this study (21 and 6 cal. kyr BP). The eustatic value varies only by a small amount for the different viscosity models due to the influence of the Earth model on the predicted area of the ocean basin as a function of time (see Eq. (2)). For example, the range of values at the LGM (when the spread is the largest) calculated for the Bassett et al. ice model is 127.10–127.43 m with a mean value of 127.24 m. We next used the ensemble of global RSL predictions to compute, on a 1° by 1° grid, the mean deviation from the (mean) eustatic value and the standard deviation of the results about this mean. The latter, which provides a measure of the sensitivity of the RSL predictions at a given location to variations in mantle viscosity and lithospheric thickness, is shown in Fig. 5 for the 21 cal. kyr BP case and Bassett et al. ice model.

As one would expect, the greatest sensitivity to variations in viscosity structure (yellow–red shaded areas) occurs where the vertical land motion due to glacio- and hydro-isostasy is large (near glaciation centres and around land areas). Any region showing a small standard deviation in Fig. 5 (2 m or less; darker blue contours) represents, in contrast, an area in which GIA predictions are insensitive to uncertainties in radial mantle viscosity structure. These regions, which include a band offshore of the southern coasts of Australia, Asia and Africa, represent an important target for field study since the associated sea-level data sets will be subject to a relatively robust GIA correction for non-eustatic effects. That is, estimates of the eustatic level at LGM (or, equivalently, the excess ice volume at this time) are commonly derived by correcting raw sea-level records for GIA-related effects (e.g. Yokoyama et al., 2000); this correction, or mapping, will be subject to less uncertainty for sites within the zone of low standard deviation.

Of course, this does not imply that the correction for GIA effects is necessarily small in this zone, only that it is relatively stationary with respect to variations in mantle viscosity, and thus the full machinery associated with GIA-induced sea-level change (e.g. Kendall et al., 2005) may be necessary to take advantage of this stationarity. An ideal site to target for RSL observation is one that shows small variability in relation to changes in the Earth model (darker blue contours in Fig. 5) *and* a small discrepancy from the eustatic value. Such sites are highlighted in Fig. 6A which plots the results in Fig. 5 only over areas in which the mean RSL prediction for 21 cal. kyr BP falls within 3 m of the (mean) eustatic value of 127.24 m. This exercise clearly further refines the choice of optimal field localities by excluding some of the zones with small variability in Fig. 5 (an example is the region offshore of southwest Africa).

The question arises as to whether conclusions based on Fig. 6A would be sensitive to the choice of ice model. To explore this issue, Fig. 6B is analogous to Fig. 6A with the exception that results for the ICE-5G ice history (and the same suite of 162 viscosity/lithosphere Earth models) are shown. Comparison of Fig. 6A and B indicates that the results are relatively insensitive to the differences between the two ice models considered. Fig. 7 shows results analogous to Fig. 6 with the exception that we focus on RSL for 6 cal. kyr BP (the two panels in Fig. 7 are limited to zones where predictions lie within 1 m of the eustatic value). Again, these two sets of predictions (based on different ice models) are broadly similar.

Predictions analogous to those in Figs. 6 and 7 but for the times 17, 13 and 9 cal. kyr BP are shown, respectively, in Supplementary Figs. 1–3 (see Appendix A). Again, the patterns are broadly similar. The largest difference, evident at 13 cal. kyr BP (Supp. Fig. 2) is most likely related to the different source distributions for Meltwater Pulse IA in each model. Based on the maps in Figs. 6 and 7 and Supp.

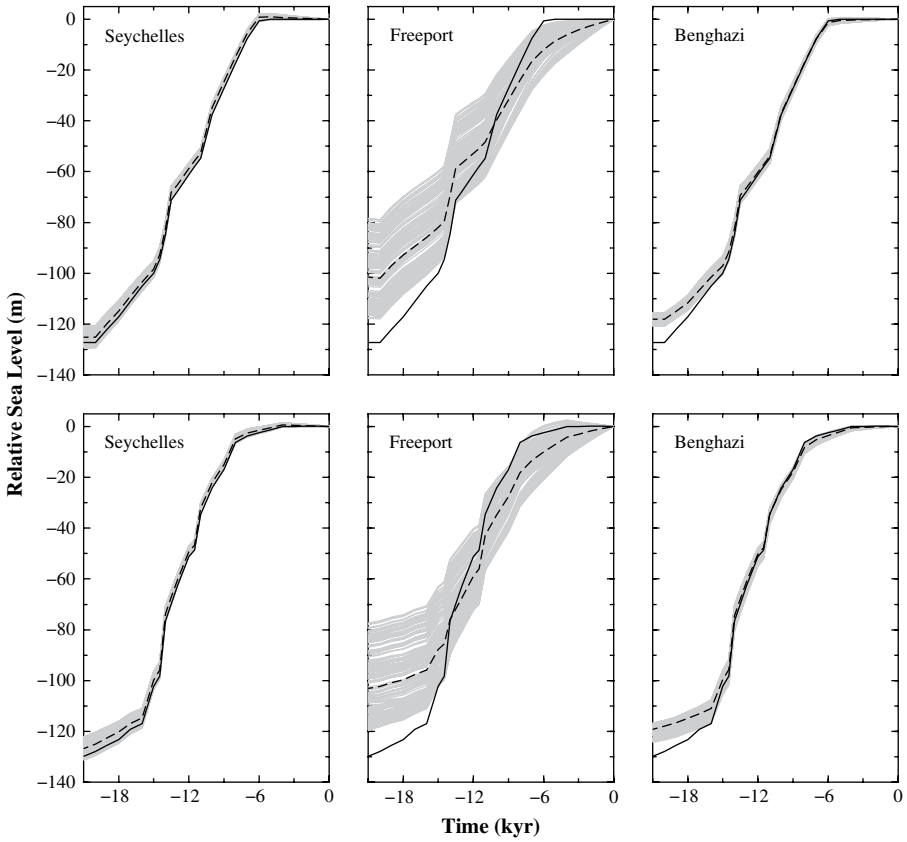

Fig. 8. Top frames show RSL predictions at three sites for the full set of 162 different Earth viscosity and lithospheric models (gray lines) and Bassett et al. ice model. The dashed and solid black lines indicate, respectively, the mean value of the predicted RSL curves and (mean) eustatic curve for this ensemble of model runs. The bottom frames show the equivalent results for the ICE-5G ice history.

Figs. 1–3, we conclude that the results shown are sensitive, mainly, to the volumetric partitioning of ice in specific regions (e.g. North America, Eurasia) and the time history of this partitioning. Spatial and temporal differences between the two models at the continent-scale – for example, the Keewatin ice dome located over central-western Canada in ICE-5G is not included in the Basset et al. model – do not appear to significantly impact the results in far-field regions.

Given the broad similarity between the two sets of ice model predictions in Figs. 6 and 7 and Supp. Figs. 1–3, we conclude that the results in these figures, which are based on an ensemble approach that considered plausible variations in Earth model parameters, can be applied with greater confidence than the results shown in Figs. 3 and 4 which are based on specific ice–Earth model pairs. We therefore propose that the maps shown in Figs. 6 and 7 (and Supp. Figs. 1–3) can serve as a useful guide to the field community for locating optimal field sites to measure RSL with an aim to constrain the eustatic component of the sea-level signal.

As a final exercise, we examine predictions of post-LGM RSL at a series of geographic sites with locations specified in Fig. 1. We begin with RSL curves at the Seychelles Islands (Indian Ocean), Freeport (Bahamas) and Benghazi (Libya), as shown in Fig. 8. Inspection of Figs. 6 and 7 indicates that RSL predictions for the Seychelles Islands lie within a few metres of the eustatic value at both the LGM (Fig. 6) and the mid-Holocene (Fig. 7) – we note that the rotational signal is small and the influence of hydro-isostasy is minor at this site. The sensitivity of these GIA results to variations in the ice and visco-elastic Earth model is also low in this area. This insensitivity is illustrated in Fig. 8, which shows the ensemble of predicted RSL curves at this locality (gray lines) as well as both the mean of these results (dashed black line) and the (mean) eustatic sea-level component (solid black line) for the Bassett et al. ice model (top frames) and the ICE-5G model (bottom frames). The small spread of the curves at 21 and 6 cal. kyr BP is a reflection of the low standard deviation predicted for this location in Figs. 6 and 7, respectively. Moreover, the predicted RSL curves for the Seychelles track the eustatic curve to within a few metres for the entire post-LGM period; we thus conclude that this would be a particularly good site for obtaining a robust time series of post-LGM eustatic sea-level change.

In contrast, an example of a poor site for this type of application would be Freeport, Bahamas. Although this site is significantly displaced from the LGM margin of the Laurentide ice sheet, it is strongly influenced by crustal motion associated with the development and collapse of a peripheral bulge. This influence is reflected in the large vertical spread of the predictions in Fig. 8, and the high values of standard deviation at this location in Figs. 6 and 7. In particular, this spread is due to the strong dependence on Earth structure of the magnitude and rate of peripheral bulge dynamics. We note also that there is a significant deviation between the predicted RSL values at Freeport and the mean eustatic value. Thus, we conclude that Freeport would be a poor site to constrain eustasy because: (i) the non-eustatic component of the signal to be removed from observations would be large for the majority of the post-LGM period, and (ii) the value of this 'correction' is highly sensitive to plausible variations in Earth viscosity structure.

The predictions for Benghazi in the southern Mediterranean show remarkably little sensitivity to the variation in Earth model parameters considered (Figs. 6–8), though there is a significant discrepancy between the predicted RSL histories and the eustatic curve in the immediate post-LGM period. Therefore, application of data from this site to infer eustatic sea level at this time would

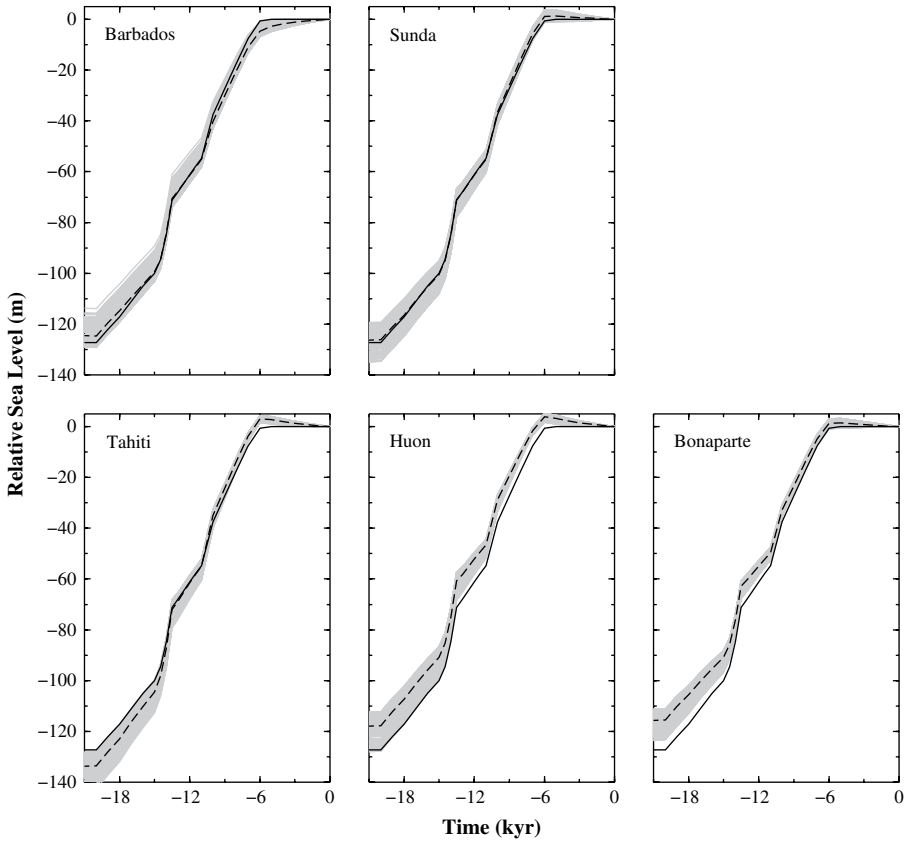

Fig. 9. Same as Fig. 8 but for five sites where long time series of RSL changes have been observed and for the Bassett et al. ice model only.

require a significant GIA correction. However, the magnitude of this correction is insensitive to Earth model parameters and so the estimate of eustasy will be relatively robust. Note, however, that from ~14 cal. kyr BP to present, the predicted mean sea-level change and the eustatic signal track each other closely, and the spread of predictions about the mean remains small.

A comparison of the predictions in Fig. 8 indicates that the two measures we use to assess the suitability of a given location for estimating the eustatic signal are similar for the two ice models considered. This similarity is also evident in Figs. 6 and 7. Not surprisingly, there are also significant differences between the predictions shown in Fig. 8 (top and bottom frames): the shape of the mean eustatic curve, which reflects the melt history of the ice model, is a good example. However, this difference is of no importance when considering the suitability of a given site for the purpose of estimating the eustatic component of sea-level change since the measures we employ are made relative to the model eustatic value.

To conclude our analysis, we show the suite of RSL predictions based on Bassett et al. model (Fig. 9) and the ICE-5G model (Fig. 10) for five far-field localities where relatively long time series of RSL have been reconstructed using various proxy indicators (Fairbanks, 1989; Bard et al., 1990, 1996; Chappell and Polach, 1991; Edwards et al., 1993; Hanebuth et al., 2000; Yokoyama et al., 2000). There is a significant sensitivity to viscosity structure at all sites. This sensitivity is most likely dominated by glacio-isostatic deformation at Barbados (i.e., peripheral bulge dynamics) and one or more of the other processes discussed above (continental levering, ocean syphoning and rotational feedback) at the remaining sites. For example, ocean syphoning is predicted to be dominant at Tahiti, and the spread of predicted RSL histories at this site is most probably related to the influence of Earth viscosity structure on this process (Mitrovica and Peltier, 1991; Mitrovica and Milne, 2002).

The magnitude, sign and time variation of the deviation between the predicted mean RSL value and the eustatic curve varies from site to site. For example, at Sunda Shelf the mean RSL curve closely tracks the eustatic value from the LGM until the present, with a particularly close accord prior to the mid-Holocene. Slightly higher discrepancies are seen at Barbados. At both Huon and Bonaparte, the modelled RSL values (and the mean curve) lie above the eustatic for the entire post-LGM period. At both these sites, the main non-eustatic signal is associated with an uplift (and sea-level fall) within a broad continental shelf due to the ocean load (i.e., continental levering); thus the departure relative to the eustatic curve will always be positive, though the amplitude of this departure will be a function of the Earth model. Finally, at Tahiti the RSL predictions (and their mean) fall below the eustatic curve prior to ~ 13 cal. Kyr BP and above this curve after ~ 11 cal. kyr BP. As discussed above, the former trend is due to the sea-level rise associated with the direct attraction of the ocean to the ablating North American ice sheets (Fig. 1A), though the range of the predictions reflects a model dependence associated with the ocean syphoning process. The change in the sign of the discrepancy at 11 cal. kyr BP is due to the sea-level fall signal associated, primarily, with ocean syphoning (Fig. 1B).

We conclude that plausible variations in viscosity can lead to an uncertainty of order 15–20 m and 4–8 m, respectively, in the mapping from RSL predictions to eustatic values at the LGM and 6 cal. kyr BP at the sites considered in Figs. 9 and 10.

3. Summary

Perturbations to the Earth's gravity field and solid surface associated with GIA cause the total (observable) sea-level change to depart from the eustatic curve. In this study we applied a state-of-the-art model of GIA-induced sea-level change to quantify the magnitude and spatial form of this departure at the

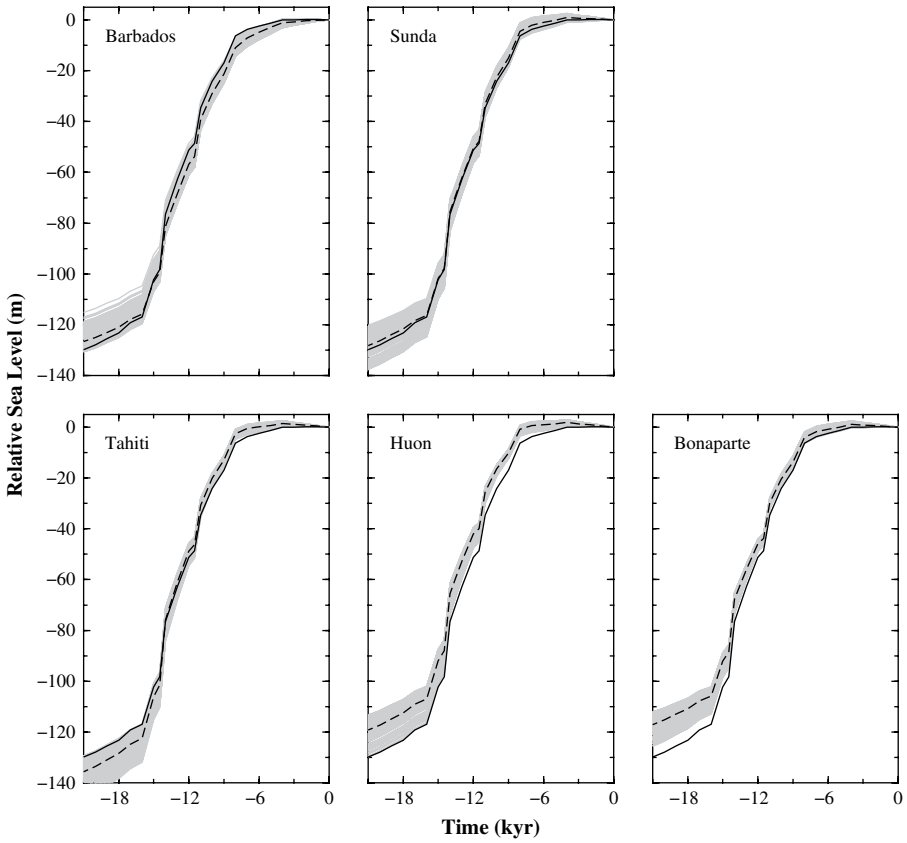

Fig. 10. Same as Fig. 9 but for the ICE-5G ice model.

global scale during the most recent deglaciation. As expected, the difference between predicted sea level and the eustatic value is largest (100s of metres) in the near-field of the ancient Late Pleistocene ice sheets, where post-glacial rebound, subsidence of the peripheral bulge and the direct attraction of the ocean to the changing ice sheets dominate the sea-level change. The departure from eustasy is also significant (10s of metres), however, in far-field regions, where various processes – ocean syphoning, continental levering, GIA-induced perturbations to Earth rotation and direct attraction – are active.

Our results indicate that, in general, eustatic sea level cannot be measured directly (Clark et al., 1978). Rather, it must be inferred by removing the non-eustatic components of the signal from observations. The accuracy of this procedure is dependent on: (1) the magnitude of the model-derived non-eustatic component and (2) the sensitivity of this correction to uncertainty in model parameters. Clearly, ideal localities for inferring eustatic sea level are those where both (1) and (2) are small. We considered two contemporary ice models and a large suite of plausible Earth models to determine locations where these criteria are best satisfied. Our results, summarised in Figs. 6 and 7, indicate that uncertainties in Earth model viscosity structure dominate those due to differences in two contemporary ice models within far-field regions. The maps shown in Figs. 6 and 7 can therefore serve as useful guides for field scientists to choose sites suitable for obtaining a relatively robust estimate of eustatic sea level at the two times considered (LGM and mid-Holocene). Maps for other times (17, 13 & 9 cal. kyr BP) are available as Supplementary on-line information (see Appendix A).

Finally, we show predictions for five sites where long time series of RSL have been observed (Barbados, Bonaparte Gulf, Huon Peninsula, Sunda Shelf and Tahiti). The uncertainty in the model correction to infer eustatic sea level from the data is in the range 15–20 m (LGM) and 4–8 m (mid-Holocene) at these sites. We note that this correction will generally be smaller for the Sunda data given that the ensemble mean bisects the spread of values and closely tracks the eustatic component for the majority of the post-LGM period. The results shown in Figs. 6 and 7 indicate that there are other sites (e.g. Seychelles, Benghazi) where the magnitude of this uncertainty can be reduced by about a factor of two or more at the LGM and mid-Holocene and so data from these sites have the potential of resulting in a more precise measure of eustatic sea level.

Acknowledgements

This work was supported by the Natural Sciences and Engineering Research Council of Canada and the Canadian Institute for Advanced Research – Earth Systems Evolution Program. This paper is a contribution to International Geological Correlation Programme Project 495 "Quaternary Land-Ocean Interactions" and the International Quaternary Association working group on "Coastal and Marine Processes." We thank Torbjörn Törnqvist and an anonymous reviewer for insightful and constructive feedback that resulted in several improvements to the original manuscript.

Appendix A. Supplementary data

Supplementary data associated with this article can be found in the on-line version, at doi:10.1016/j.quascirev.2008.08.018.

References

Bard, E., Hamelin, B., Fairbanks, R.G., Zindler, A., 1990. Calibration of the ^{14}C timescale over the past 30,000 years using mass spectrometric U–Th ages from Barbados corals. Nature 345, 405–410.

Bard, E., Hamelin, B., Arnold, M., Montaggioni, L., Cabioch, G., Faure, G., Rougerie, F., 1996. Deglacial sea-level record from Tahiti corals and the timing of global meltwater discharge. Nature 382, 241–244.

Bassett, S.E., Milne, G.A., Mitrovica, J.X., Clark, P.U., 2005. Ice sheet and solid earth influences on far-field sea-level histories. Science 309, 925–928.

Bloom, A.L., 1967. Pleistocene shorelines: a new test of isostasy. Geol. Soc. Am. Bull. 78, 1477–1494.

Chappell, J., 1971. Late Quaternary glacio- and hydro-isostasy, on a layered earth. Quat. Res. 4, 429–440.

Chappell, J., Polach, H., 1991. Post-glacial sea-level rise from a coral record at Huon Peninsula, Papua New Guinea. Nature 349, 147–149.

Clark, J.A., 1976. Greenland's rapid postglacial emergence: a result of ice-water gravitational attraction. Geology 4, 310–312.

Clark, J.A., Farrell, W.E., Peltier, W.R., 1978. Global changes in postglacial sea level: a numerical calculation. Quat. Res. 9, 265–287.

Clark, P.U., Mix, A.C., 2002. Ice sheets and sea level of the Last Glacial Maximum. Quatern. Sci. Rev. 21, 1–7.

Clark, P.U., Mitrovica, J.X., Milne, G.A., Tamisiea, M., 2002. Sea-level fingerprinting as a direct test for the source of global meltwater pulse 1A. Science 295, 2438–2441.

Daly, R.A., 1925. Pleistocene changes of level. Am. J. Sci. 10, 281–313.

Dziewonski, A.M., Anderson, D.L., 1981. Preliminary reference earth model (PREM). Phys. Earth Planet. Inter. 25, 297–356.

Edwards, R.L., Beck, J.W., Burr, G.S., Donahue, D.J., Chappell, J.M.A., Bloom, A.L., Druffel, E.R.M., Taylor, F.W., 1993. A large drop in atmospheric $^{14}C/^{12}C$ and reduced melting in the Younger Dryas, documented with ^{230}Th ages of corals. Science 260, 962–968.

Fairbanks, R.G., 1989. A 17,000-year glacio-eustatic sea level record: influence of glacial melting rates on the Younger Dryas event and deep-ocean circulation. Nature 342, 637–642.

Farrell, W.E., Clark, J.A., 1976. On postglacial sea-level. Geophys. J. R. Astr. Soc. 46, 647–667.

Fleming, K., Johnston, P., Zwartz, D., Yokoyama, Y., Lambeck, K., Chappell, J., 1998. Refining the eustatic sea-level curve since the Last Glacial Maximum using far- and intermediate-field sites. Earth and Planetary Science Letters 163, 327–342.

Hanebuth, T., Stattegger, K., Grootes, P.M., 2000. Rapid flooding of the Sunda Shelf: a Late-Glacial sea-level record. Science 288, 1033–1035.

Haskell, N.A., 1935. The motion of a fluid under a surface load, 1. Physics 6, 265–269.

Johnston, P., 1993. The effect of spatially non-uniform water loads on predictions of sea level change. Geophys. J. Int. 114, 615–634.

Kaufmann, G., Lambeck, K., 2002. Glacial isostatic adjustment and the radial viscosity profile form inverse modelling. J. Geophys. Res. 107, doi:10.1029/2001JB000941.

Kendall, R., Mitrovica, J.X., Milne, G.A., 2005. On post-glacial sea level - II. Numerical formulation and comparative results on spherically symmetric models. Geophys. J. Int. 161, 679–706.

Lambeck, K., 1993. Glacial rebound of the British Isles - II. A high resolution, high-precision model. Geophys. J. Int. 115, 960–990.

Lambeck, K., 2002. Sea level change from mid-Holocene to recent time: an Australian example with global implications in Glacial isostatic adjustment and the earth system: sea level, crustal deformation, gravity and rotation. In: Mitrovica, J.X., Vermeersen, L.L.A. (Eds.), AGU monograph, Geodynamics Series, vol. 29, pp. 33–50.

Lambeck, K., Smither, C., Johnston, P., 1998. Sea-level change, glacial rebound and mantle viscosity for northern Europe. Geophys. J. Intern. 134, 102–144.

Lambeck, K., Yokoyama, Y., Johnston, P., Purcell, A., 2000. Global ice volumes at the Last Glacial Maximum. Earth Planet. Sci. Lett. 181, 513–527.

Lambeck, K., Yokoyama, Y., Purcell, A., 2002. Into and out of the Last Glacial Maximum: sea-level change during Oxygen Isotope Stages 3 and 2. Quatern. Sci. Rev. 21, 343–360.

Lambeck, K., Anzidei, M., Antonioli, F., Benini, A., Esposito, E., 2004. Sea level in Roman time in the central Mediterranean and implications for modern sea level rise. Earth Planet. Sci. Lett. 224, 563–575.

Milliman, J.D., Emery, K.O., 1968. Sea levels during the past 35,000 years. Science 162, 1121–1123.

Milne, G.A., 1998. Refining models of the glacial isostatic adjustment process. PhD thesis, University of Toronto, pp. 1–123.

Milne, G.A., 2002. Recent advances in predicting glaciation-induced sea-level changes and their impact on model applications in glacial isostatic adjustment and the earth system: sea level, crustal deformation, gravity and rotation. In: Mitrovica, J.X., Vermeersen, L.L.A. (Eds.), AGU monograph, Geodynamics Series, vol. 29, pp. 157–176.

Milne, G.A., Mitrovica, J.X., 1996. Postglacial sea-level change on a rotating earth: first results from a gravitationally self-consistent sea-level equation. Geophys. J. Int. 126, F1–F8.

Milne, G.A., Mitrovica, J.X., 1998. Postglacial sea-level change on a rotating Earth's. Geophys. J. Int. 133, 1–19.

Milne, G.A., Mitrovica, J.X., Davis, J.L., 1999. Near-field hydro-isostasy: the implementation of a revised sea-level equation. Geophys. J. Int. 139, 464–483.

Milne, G.A., Mitrovica, J.X., Schrag, D.P., 2002. Estimating past continental ice volume from sea-level data. Quat. Sci. Rev. 21, 361–376.

Milne, G.A., Long, A.J., Bassett, S.E., 2005. Modelling Holocene relative sea-level observations from the Caribbean and South America. Quat. Sci. Rev. 24, 1183–1202.

Mitrovica, J.X., 1996. Haskell [1935] revisited. J. Geophys. Res. 101, 555–569.

Mitrovica, J.X., Forte, A.M., 2004. A new inference of mantle viscosity based upon joint inversion of convection and glacial isostatic adjustment data. Earth Planet. Sci. Lett. 225, 177–189.

Mitrovica, J.X., Milne, G.A., 2002. On the origin of postglacial ocean syphoning. Quat. Sci. Rev. 21, 2179–2190.

Mitrovica, J.X., Milne, G.A., 2003. On post-glacial sea level - I. General theory. Geophys. J. Int. 154, 253–267.
Mitrovica, J.X., Peltier, W.R., 1991. On post-glacial geoid subsidence over the equatorial oceans. J. Geophys. Res. 96, 20053–20071.
Mitrovica, J.X., Peltier, W.R., 1993. A new formalism for inferring mantle viscosity based on estimates of post-glacial decay times: application to RSL variations in N.E. Hudson Bay. Geophys. Res. Lett. 20, 2183–2186.
Mitrovica, J.X., Tamiseia, M.E., Davis, J.L., Milne, G.A., 2001. Recent mass balance of polar ice sheets inferred from patterns of global sea-level change. Nature 409, 1026–1029.
Mitrovica, J.X., Wahr, J., Matsuyama, I., Paulson, A., 2005. The rotational stability of an ice-age earth. Geophys. J. Int. 161, 491–506.
Nakada, M., Lambeck, K., 1989. Late Pleistocene and Holocene sea-level change in the Australian region and mantle rheology. Geophys. J. Int. 96, 497–517.
Peltier, W.R., 1994. Ice age paleotopography. Science 265, 195–201.
Peltier, W.R., 1998. Postglacial variations in the level of the sea: implications for climate dynamics and solid-earth geophysics. Rev. Geophys. 36, 603–689.
Peltier, W.R., 2002. On eustatic sea level history: Last Glacial Maximum to Holocene. Quat. Sci. Rev. 21, 377–396.
Peltier, W.R., 2004. Global glacial isostasy and the surface of the ice-age earth: The ICE-5G (VM2) model and GRACE. Annu. Rev Earth Planet. Sci. 32, 111.
Peltier, W.R., Andrews, J.T., 1976. Glacial isostatic adjustment–I. The forward problem. Geophys. J. R. Astr. Soc. 46, 605–646.
Peltier, W.R., Fairbanks, R.G., 2006. Global glacial ice volume and Last Glacial Maximum duration from an extended Barbados sea level record. Quat. Sci. Rev. 25, 3322–3337.
van de Plassche O. 1986. Sea-level research: a manual for the collection and evaluation of data. GeoBooks, Norwich.
Sabadini, R., Yuen, D.A., Boschi, E., 1982. Polar wander and the forced responses of a rotating, multi-layered, viscoelastic planet. J. Geophys. Res. 87, 2885–2903.
Shennan, I., Peltier, W.R., Drummond, R., Horton, B.P., 2002. Global to local scale parameters determining relative sea-level changes and the post-glacial isostatic adjustment of Great Britain. Quat. Sci. Rev. 21, 397–408.
Tushingham, A.M., PeltierPeltier, W.R., 1991. ICE-3G: a new global model of late Pleistocene deglaciation based on geophysical predictions of post-glacial relative sea level change. J. Geophys. Res. 96, 4497–4523.
Woodward, R.S., 1888. On the form and position of mean sea level. US Geol. Surv. Bull. 48, 87–170.
Wu, P., Peltier, W.R., 1983. Glacial isostatic adjustment and the free air gravity anomaly as a constraint on deep mantle viscosity. Geophys. J. R. Astr. Soc. 74, 377–449.
Wu, P., Peltier, W.R., 1984. Pleistocene deglaciation and the Earth's rotation: a new analysis. Geophys. J. R. Astr. Soc. 76, 753–792.
Yokoyama, Y., Lambeck, K., De Deckker, P., Johnston, P., Fifield, L.K., 2000. Timing of the Last Glacial Maximum from observed sea-level minima. Nature 406, 713–716.